Title

Effect of montmorillonite K10 clay on RNA structure and function.

Journal

Biophysical Journal, 123(4)

Authors

Saha, Ranajay
Kao, Wei-Ling
Malady, Brandon
et al.

Publication Date

2024-02-20

DOI

10.1016/j.bpj.2023.11.002

Peer reviewed

Biophysical Journal
Article

Biophysical Society

Effect of montmorillonite K10 clay on RNA structure and function

Ranajay Saha,[1,2] Wei-Ling Kao,[3] Brandon Malady,[2] Xiao Heng,[3] and Irene A. Chen[1,2,*]
[1]Department of Chemical and Biomolecular Engineering, Department of Chemistry and Biochemistry, University of California, Los Angeles, California; [2]Department of Chemistry and Biochemistry, University of California, Santa Barbara, California; and [3]Department of Biochemistry, University of Missouri, Columbia, Missouri

ABSTRACT One of the earliest living systems was likely based on RNA ("the RNA world"). Mineral surfaces have been postulated to be an important environment for the prebiotic chemistry of RNA. In addition to adsorbing RNA and thus potentially reducing the chance of parasitic takeover through limited diffusion, minerals have been shown to promote a range of processes related to the emergence of life, including RNA polymerization, peptide bond formation, and self-assembly of vesicles. In addition, self-cleaving ribozymes have been shown to retain activity when adsorbed to the clay mineral montmorillonite. However, simulation studies suggest that adsorption to minerals is likely to interfere with RNA folding and, thus, function. To further evaluate the plausibility of a mineral-adsorbed RNA world, here we studied the effect of the synthetic clay montmorillonite K10 on the malachite green RNA aptamer, including binding of the clay to malachite green and RNA, as well as on the formation of secondary structures in model RNA and DNA oligonucleotides. We evaluated the fluorescence of the aptamer complex, adsorption to the mineral, melting curves, Förster resonance energy transfer interactions, and ^{1}H-NMR signals to study the folding and functionality of these nucleic acids. Our results indicate that while some base pairings are unperturbed, the overall folding and binding of the malachite green aptamer are substantially disrupted by montmorillonite. These findings suggest that minerals would constrain the structures, and possibly the functions, available to an adsorbed RNA world.

SIGNIFICANCE Life on earth is believed to have progressed through an intermediate stage in which RNA took on multiple roles, including genetic material and biocatalysts. It has been suggested that certain clay minerals, such as montmorillonite, may have facilitated the emergence of RNA-based life by promoting chemical processes and enforcing spatial segregation that limited the spread of parasitic sequences. At the same time, interactions between a mineral surface and adsorbed RNA are expected to perturb RNA structure and function. Here we studied the effect of montmorillonite on the folding of model oligonucleotides, including an aptamer. While some base-pairing interactions were preserved, tertiary structure and function were disrupted by montmorillonite. The results indicate that mineral association would constrain an RNA world.

INTRODUCTION

The establishment of RNA as a genetic and functional molecule, heralding the "RNA world," is hypothesized to have been a critical transition during the origin of life (1–7). The emergence of RNA would require at least the abiotic provision of activated nucleotide building blocks (8,9), polymerization of nucleotides to create ribozyme or aptamer sequences capable of exhibiting chemical activity (10–13), and the generation of folded, functional forms. However, probable niches for RNA that would support its survival and activity are not understood well. The effects of environmental conditions such as metal ions, temperature, pH, pressure, freezing, and dehydration on ribozyme catalysis were recently reviewed (14). Intriguingly, the involvement of clay minerals has been suggested to facilitate multiple prebiotic processes. From a theoretical evolutionary perspective, surface attachment can provide a solution to the problem of parasites in a cooperative system, as individual locales on the surface form groups that are relatively insulated from parasitic invasion (15). Surfaces may thus provide an alternative to cell-based life, in which a conceptually similar resistance to parasitism is achieved through compartmentalization (16).

Submitted October 5, 2022, and accepted for publication November 1, 2023.
*Correspondence: ireneachen@ucla.edu
Editor: Jason Kahn.
https://doi.org/10.1016/j.bpj.2023.11.002

Minerals, particularly clays, can adsorb nucleobases, nucleosides, nucleotides, and RNA, depending on the clay itself as well as a variety of environmental factors including pH, temperature, and cation concentrations (17). Interestingly, longer RNA molecules have been observed to be preferentially bound to the minerals hydroxyapatite, pyrite, pyrrhotite, magnetite, and calcite (18). The interactions of nucleotides with minerals are complex (17,19–21). For the smectite clay minerals montmorillonite and nontronite, two types of interactions with mononucleotides are observed, namely ligand exchange of -OH groups on the clay edge surfaces with the phosphates of the nucleotides and cation-mediated interactions between the nitrogenous base and the negatively charged basal plane (20). Montmorillonite is a smectite clay consisting of sheets of silica sandwiching alumina, with sheets being separated by a cationic hydration layer (17). The lattice includes a triple-sheet structure, with an aluminum-oxygen and aluminum-hydroxyl octahedral sheet sandwiched between two silicon-oxygen tetrahedral sheets. The layers of the triplet sheet are associated by van der Waals forces (22), and the interlayers consist of water and substitutable metal ions (e.g., K^+). Although RNA is negatively charged, both anionic and cationic clay minerals are known to bind RNA. For negatively charged mineral surfaces, cations in solution are required to neutralize the charges, with divalent cations being more effective than monovalent cations (23). Perhaps counterintuitively, in studies of the clay montmorillonite, the sites of interaction on the RNA appear to be the nucleobases rather than the backbone, based on molecular dynamics simulation (24). Nitrogen-containing groups appear to be implicated in the adsorption of adenosine and 5′-adenosine monophosphate to montmorillonite, based on infrared spectroscopy (25). In simulations, RNA constructs, including a hammerhead ribozyme and an RNA duplex, are predicted to bind the mineral surface via a single, tethered terminal base, which is bound through a combination of van der Waals and electrostatic interactions. Thus, under chemical conditions supporting these interactions (17,26,27), a substantial fraction of RNAs in a prebiotic milieu in which minerals are present might be expected to be adsorbed.

In addition to exhibiting stable adsorption of RNA, clay minerals, particularly the phyllosilicate montmorillonite, have attracted considerable attention for its additional properties relevant to the prebiotic emergence of RNA. Clay minerals are ubiquitous on our planet, with more than 33 different minerals thought to be present during the Hadean and early Archean when life originated (28), although the physical and chemical properties of specific clays may or may not be relevant to an RNA world. Their prebiotic presence is supported by the observation of minerals that appear to be derived from clay on Mars greater than 3.5 billion years old (29). A variety of minerals, including montmorillonite, and other surfaces have also been found to catalyze the self-assembly of vesicles from fatty acids, suggesting a possible route for transition from a surface-associated system to a compartmentalized system (30). Interestingly, photocatalytic minerals present in extracellular vesicles can utilize light energy to drive a multistep transmembrane electron transfer reaction, resulting in the generation of a proton gradient (31), demonstrating the potential for a protometabolic pathway in a mixed mineral-vesicle system. A surface-mediated scenario for the origin of life (32) has been studied experimentally in terms of the chemical processes that minerals can facilitate. Mineral surfaces have been found to concentrate prebiotic building blocks and act as heterogeneous catalysts (33,34). For example, minerals can concentrate, align, and act as adsorption templates for amino acids and promote abiotic peptide bond formation (35). Thus, minerals have attracted significant attention as a potential local environment for prebiotic processes.

With respect to RNA, montmorillonite has been extensively studied for its ability to catalyze RNA polymerization from imidazolide-activated nucleotides (36–40), resulting in RNA oligomers as long as some aptamers and ribozymes (up to approximately 50-mers). Based on comparison with zincite, interactions between the montmorillonite surface and the nitrogenous bases, rather than the phosphates, appear to be important for catalyzing RNA polymerization (21). Furthermore, prebiotically plausible α-amino acids may act as coenzymes in enhancing montmorillonite-catalyzed RNA polymerization in an Mg^{2+}-independent mechanism, compatible with protocell stability (41). Other prebiotically feasible minerals, namely amorphous and crystalline quartz and mica, have been reported to host the polymerization of 3′,5′ cyclic GMP, although calcite, olivine, and serpentine-group minerals did not, possibly due to their basic nature (42). At the same time, RNA polymers are also stabilized against nonspecific degradation. UV radiation would have been an important prebiotic source of chemical damage to RNA, particularly in active sites, single-stranded regions, and random coil structures (43,44). Adenosine and RNA adsorbed by montmorillonite appear to be protected from radiation damage (45); for example, a self-cleaving ADHR1 ribozyme in the presence of montmorillonite was three times more resistant to UV damage than ribozyme lacking the mineral (46). Mineral-adsorbed RNAs can also persist in the presence of degrading agents and retain the ability to template enzymatic reactions such as RT-PCR, albeit with reduced efficiency and processivity (47). Thus, mineral adsorption could support both RNA synthesis and survival in the physical environment (relevant studies are summarized in Table S1).

Despite these favorable features of minerals, particularly montmorillonite, for an RNA world it is unclear whether RNA sequences could retain complex folding and chemical activities on minerals. On one hand, some experimental and theoretical studies suggest that at least some RNA folds and activities are stable when bound to montmorillonite. Molecular dynamics simulations showed that a duplex remains

intact while tethered to the surface via a single terminal base (24). Experimental studies confirmed that poly(A) retained the ability to complex with poly(U) and that an adsorbed RNA was still capable of acting as a template for RT-PCR (47), indicating that duplex formation was possible. In addition, studies of the hammerhead ribozyme showed measurable self-cleavage efficiency on montmorillonite, although the activity was reduced to 20%, possibly due to reduced mobility after adsorption (48). Higher amounts of montmorillonite lead to greater inhibition (up to a 30-fold drop in activity at 50 mg/mL of clay) (49). Consistent with the studies on duplex formation, the hammerhead ribozyme also retained the ability to anneal to an oligonucleotide that promoted activity (48). A systematic comparison of two parallel *in vitro* selections for self-cleaving ribozymes, performed in the presence or absence of montmorillonite, showed little difference in the outcome. While the presence of the clay inhibited the ribozymes somewhat, consistent with the earlier results on the hammerhead ribozyme, the *in vitro* selection study indicated that montmorillonite did not affect the overall fitness landscape of the RNAs (50). These studies suggest that montmorillonite does not greatly perturb the RNA, at least with respect to duplex formation or self-cleavage activity.

On the other hand, molecular dynamics simulations also predict that three-dimensional folding would be significantly altered by the presence of montmorillonite (51). Unlike free aqueous solution, which accommodates extended conformations and exploration of conformational space, montmorillonite appears to cause rapid compaction of the RNA into a globular form, analogous to a "molten globule" in protein folding. RNA compaction upon attachment to a surface is consistent with the excluded volume effects, including from macromolecular crowding and confinement in vesicles, which have been previously observed in multiple RNA systems (52–54). Such effects can stabilize intermolecular associations and structure formation and indirectly promote evolutionary adaptation (53,55,56). In simulations with montmorillonite, these effects may have a positive or negative effect on native folding, as the metastable compacted globule, which is stabilized by hydrogen bonding and suboptimally folded substructures, may then undergo a slow rearrangement to a folded or misfolded state (24). In contrast, such metastable states appear to be lacking in simulations in bulk water. Molecular dynamics simulations of the hammerhead ribozyme, in particular, showed a compacted ribozyme that excluded Mg^{2+} from the active site, closing the catalytic pocket such that an alternative, Mg^{2+}-independent mechanism for self-cleavage would be adopted (51), possibly explaining the slower rate observed experimentally (48). These considerations suggest that although self-cleaving ribozymes appear to be relatively tolerant of montmorillonite, other functional RNAs might be prominently affected by interaction of the RNA with montmorillonite (e.g., if the tertiary folds are sensitive to compaction, significant misfolded structures exist, or the activities lack alternative mechanisms available to a compacted state).

In the present work, we studied how montmorillonite affected the folding and function of the malachite green RNA aptamer, which binds to and increases the fluorescence of the small molecule malachite green by approximately 2360-fold by restricting its vibrational deexcitation (57). A synthetic mineral, montmorillonite K10 ($(K_{0.25}Na_{0.118}Ca_{0.022})(Al_{1.06}Fe_{0.206}Mg_{0.166})(Si_{7.39}Al_{0.61})O_{20}(OH)_4$),which is not naturally occurring, was used, since the higher homogeneity would allow greater uniformity in the interactions compared to natural clay samples (58). In addition to monitoring aptamer adsorption, activity, and folding, we also studied three model nucleic acid systems (an RNA duplex, a DNA duplex, and a DNA hairpin structure) to probe adsorption and the effect of montmorillonite on their structural stability. The results indicate that the tertiary structure and function of the aptamer, but not certain secondary structures or duplexes, were substantially perturbed by montmorillonite. These studies expand our understanding of how the presence of montmorillonite might affect the emergence of an RNA world.

MATERIALS AND METHODS

Materials

Malachite green (MG) chloride from Sigma-Aldrich was used as received. The MG aptamer RNA (5′-GGA UCC CGA CUG GCG AGA GCC AGG UAA CGA AUG GAU CC-3′), hairpin DNA (5′-/5′ fluorescein dT/GG AAT GGA ATT TTT ATT CC/i6-TAMRA/ATT CC-3′), RNA hybrid sequences (5′-/5′ fluorescein dT/GG AAU GGA AU-3′ (donor RNA strand), 5′-AUU CC/i6-TAMRA/AUU CC-3′ (acceptor RNA strand)), and DNA hybrid sequences (5′-/5′ fluorescein dT/GG AAT GGA AT-3′ (donor DNA strand), 5′-ATT CC/i6-TAMRA/ATT CC-3′ (acceptor DNA strand)) labeled with paired Förster resonance energy transfer (FRET) dyes were obtained by chemical synthesis and HPLC-purified by IDT (San Diego, CA). MG aptamer was fluorescently labeled using a 5′ EndTag DNA/RNA Labeling Kit (Vector Laboratories, Newark, CA) and either fluorescein maleimide (TCI Chemicals, Tokyo, Japan) or Alexa Fluor 647 C_2 maleimide (Thermo Fisher Invitrogen, Waltham, MA). Other chemicals not mentioned above were purchased from Fisher Scientific (Waltham, MA).

Preparation of montmorillonite stock suspension

Isolation of fine particles of montmorillonite K10 (Sigma, St. Louis, MO) was performed according to a previous report (30). To remove large particles, 5 g of the sample was added to 45 mL Milli-Q water, mixed by vortexing, and allowed to settle for 1 h. Approximately 30 mL of the supernatant suspension of montmorillonite was then removed to a new tube and centrifuged at 5000 × *g* for 30 min. The supernatant was discarded, and 45 mL of 100% ethanol was used to disperse the pellet. Centrifugation (at 5000 × *g*, 30 min) of the dispersion allowed pelleting of the fine particles of montmorillonite. The supernatant was discarded, and the pellet was dried overnight using a lyophilizer. A stock suspension of 50 mg/mL montmorillonite particles was prepared in Milli-Q water.

Preparation of oligonucleotide solutions with montmorillonite

The DNA or RNA stock solutions (2 μM in 50–200 μL of 2.5–5 mM Tris-Cl, pH 8.5) were heated to 90°C for 3 min and cooled on ice for 10 min. The cooled RNA solutions were added to buffer and salt solutions to obtain a final concentration of 0.2 μM RNA in 0.25–3.3 mM Tris, 10 mM HEPES, 1 mM Mg-citrate, 100 mM KCl, 0.2 M bicine, pH 8.5, with a specific amount of montmorillonite added. For DNA, the final solution contained 0.2 μM DNA in either buffer containing $MgCl_2$ (0.25–3.3 mM Tris, 1 mM $MgCl_2$, 15 mM KCl, 0.2 M bicine, pH 8.5) or buffer containing Mg-citrate (3.0 mM Tris, 10 mM HEPES, 1 mM Mg-citrate, 100 mM KCl, 0.2 M bicine, pH 8.5) in the presence of a specific amount of montmorillonite. The solutions were tumbled overnight. To assess whether RNA adsorbed onto montmorillonite was able to hybridize, the donor strands were initially mixed with montmorillonite and tumbled overnight, after which the acceptor RNA strand was added, followed by overnight tumbling.

For experiments including MG, MG was added after overnight tumbling of montmorillonite with RNA followed by additional tumbling for at least 6 h to achieve equilibration of the dye (Fig. S1). Fluorescence of the supernatant after centrifugation (5000 × *g*, 30 min) or the bulk solution was recorded using a Fluoromax 4c (Horiba, Kyoto, Japan) or a Tecan (Männedorf, Switzerland) M200 Pro plate reader (λ_{ex} = 617 nm and λ_{em} = 660 nm).

Quantification of RNA release from montmorillonite

5′-Alexa 647-labeled 0.2 μM MG aptamer (folded in 0.5 mM Tris, 10 mM HEPES, 1 mM Mg-citrate, 100 mM KCl, 0.2 M bicine, pH 8.5) was mixed with and without montmorillonite (1 mg/mL) and was tumbled overnight (1 mL total solution). The next day, the whole solution was centrifuged (14,000 rpm, 15 min), supernatant was removed through filtration (with 0.2 μm centrifugal filter), and the pellet was washed with 100 μL of buffer. The amount of bound RNA fluorescence (F_b) was calculated from the supernatant fluorescence (F_{sup}) (unbound RNA) compared to the total RNA fluorescence F_0 (measured before addition of montmorillonite) ($F_b = F_0 - F_{sup}$). Subsequently the pellet was dispersed in 1 mL of buffer for RNA desorption, and the fluorescence of the supernatant (F_t, after centrifugation at 14,000 rpm, 15 min) was checked (day 1). The supernatant was returned to the stock solution and tumbled overnight, and supernatant fluorescence was similarly checked for RNA release on day 2 and so on. The bound fraction released (F_{rel}) was calculated from F_t according to $F_{rel} = F_t/F_b$.

Measurement of binding of oligonucleotides to montmorillonite

Montmorillonite was mixed with the DNA or RNA oligonucleotide (with Alexa Fluor 647, fluorescein, or TAMRA label) as described above, and the bound fraction (f_b) of the oligonucleotide after overnight mixing was calculated as $1 - F_{sup}/F_0$, where F_{sup} is the fluorescence of the supernatant after centrifugation (5000 × *g*, 30 min) and F_0 is the fluorescence of the montmorillonite-free solution. The bound fraction of an oligo measured over the range of experimental montmorillonite concentrations (0–30 mg/mL) yielded a binding isotherm. The curves were fitted to a linear form using the following equation (59):

$$\frac{M}{F_b} = \frac{M}{F_\infty} + \frac{1}{K_a \times F_\infty},$$

where M is the montmorillonite concentration (mg/mL), F_b is the bound fluorescence ($F_b = f_b \times F_0$) at a given montmorillonite concentration, F_∞ is the fluorescence at binding saturation with montmorillonite, and K_a is the apparent equilibrium binding constant. The linear fit of the graph (M/F_b vs. M) yields parameters F_∞ from the slope (slope = $1/F_\infty$) and K_a from the intercept (intercept = $1/(K_a \times F_\infty)$). Direct nonlinear fitting used the equation $f_b = f_{max} \frac{M}{K_D+M}$. For first-order adsorption, the relationship for apparent $K_D = 1/K_a$ was used.

Melting curves of FRET-labeled oligonucleotides

The ratio of donor-to-acceptor fluorescence (λ_{ex} = 450 nm, donor λ_{em} = 520 nm, acceptor λ_{em} = 585 nm) of either the DNA hairpin (0.2 μM) or the duplex DNA or RNA (0.2 μM donor to 0.4 μM acceptor strand), in the presence or absence of 10 mg/mL montmorillonite, was recorded while stirring. Measurements were taken in 2°C–3°C increments from 1°C to 92°C, with a 5-min incubation at each interval (Fluoromax 4C with Peltier attachment, described below). Fluorescence intensity ratios (F_{520}/F_{585}) were normalized to minimum of 0 and a maximum of 1. Melting curves were fitted in Origin Pro 2015 software using the Boltzmann sigmoidal equation $\frac{F_{520}}{F_{585}} = A_{min} + (A_{max} - A_{min})/(1 + \exp(\frac{T - T_m}{s}))$, where F refers to fluorescence and A_{min} and A_{max} are the minimum and maximum fluorescence ratios, respectively, T is temperature, T_m is the melting temperature, and s is a fitting parameter (slope to allow fitting of cooperative transitions) (60).

Melting transition of the MG aptamer

The fluorescence of the MG aptamer was measured at different temperatures using a Fluoromax 4C (Horiba) with a Peltier-controlled temperature attachment (Model F-3004, Horiba). The fluorescence of the aptamer-dye complex (0.2 μM MG RNA and 12 μM MG dye) in presence (1 mg/mL) and absence of montmorillonite was recorded while stirring, in 3°C increments from 1°C to 70°C, with a 5-min incubation at each interval. Fluorescence intensities for MG (λ_{ex} = 617 nm, λ_{em} = 660 nm) were recorded and normalized to a minimum of 0 and a maximum of 1. As in the previous section, melting curves were fitted in Origin Pro 2015 software using the Boltzmann sigmoidal equation

$$F = F_{min} + (F_{max} - F_{min}) \Big/ \left(1 + exp\left(\frac{T - T_t}{s}\right)\right),$$

where F refers to fluorescence and F_{min} and F_{max} are the minimum and maximum fluorescence, respectively, T is temperature, T_t is the transition temperature, and s is a fitting parameter.

FRET measurement of MG-aptamer folding

The MG aptamer was 5′-labeled by fluorescein maleimide using the DNA/RNA labeling kit from Vector Laboratories. The RNA aptamer solutions were folded in 3.3 mM Tris, 10 mM HEPES, 1 mM Mg-citrate, 100 mM KCl, 0.2 M bicine, pH 8.5, with a concentration of montmorillonite of 1 mg/mL. The 5′-labeled fluorescein-RNA (1.05 μM) was excited at 480 nm, and the steady-state fluorescence was monitored at 519 nm using a Fluoromax 4C (Horiba), in the presence (F^{DA}) or absence (F^{D}) of the acceptor dye (23.6 μM MG). The FRET efficiency (E) was estimated using the following equation (61):

$$E = 1 - \frac{F^{DA}}{F^{D}}.$$

NMR of the MG aptamer

The MG aptamer RNA used in NMR spectroscopy was synthesized by *in vitro* T7 transcription reactions using the synthesized DNA template

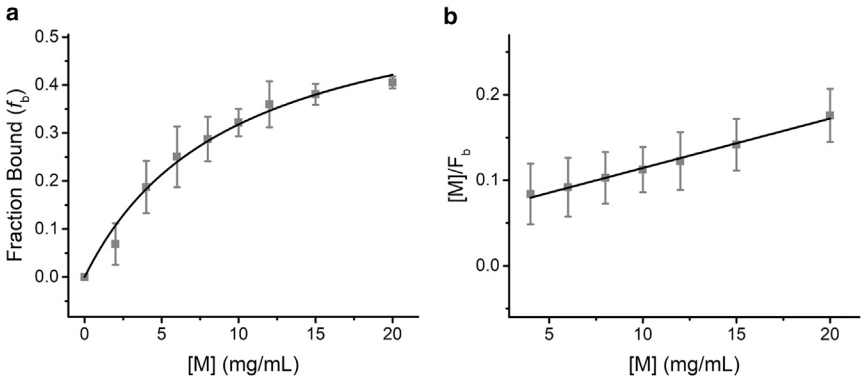

FIGURE 1 Adsorption of MG aptamer onto montmorillonite. (*a*) Fluorescence of 5′-labeled MG aptamer showing increasing fraction of bound RNA (f_b) with montmorillonite concentration. Data were fit directly to a binding curve (apparent K_a = 0.11 ± 0.05 mL/mg; apparent K_D = 9.1 mg/mL) (adj. R^2 = 0.98). (*b*) The linearized plot according to the Langmuir model, plotted with respect to the montmorillonite concentration (F_b denotes bound fluorescence; *M* denotes montmorillonite). From linear fitting, apparent K_a = 0.13 ± 0.06 mL/mg, apparent K_D = 7.7 mg/mL (adj. R^2 = 0.996). Error bars represent standard deviation of three independent experiments (N = 3).

5′-GGT ACC ATT CG TTA CCT GGC TCT CGC CAG TCG GG TAC CTA TAG TGA GTC GTA TTA ATT TC-3′ annealed to 5′-GAA ATT AAT ACG ACT CAC TAT A-3’ (IDT). The underlined sequence denotes the T7 promoter sequence. The MG-aptamer sequence was chosen to allow matching of specific resonances to previously published data (62). The *in vitro* RNA synthesis was carried out at 37°C for 3 h in an 18-mL reaction solution containing 40 mM Tris-HCl (pH 8.0), 5 mM dithiothreitol, 10 mM spermidine, 0.01% Triton X-100, 25 mM $MgCl_2$, 20 μL of RNase inhibitor (40 U), 0.05% dimethyl sulfoxide, and 1 mM NTP. The reaction was quenched with 25 mM EDTA and 1 M urea, mixed with 10% glycerol, and run on 15% denaturing acrylamide gels at 16 W overnight. RNA was visualized by UV light, extracted from the gel through electroelution (Elutrap; Whatman, Little Chalfont, UK), and washed in Amicon ultracentrifugal filters.

The MG-aptamer samples were prepared (200–300 μM) and prefolded by heating in 10 mM dTris-HCl, pH 7.5 at 90°C for 3 min and cooling on ice for 10 min. The folding buffer was added into the RNA sample to reach the final concentration of 200 μM RNA, 10 mM dTris-HCl (pH 7.5), 1 mM $MgCl_2$, and 100 mM KCl. The RNA solution was then incubated with equimolar of MG at 37°C for 30 min, 0.4–4 mg/mL montmorillonite slurry was titrated into the RNA:MG mixture, and 1D ^{1}H-NMR spectra were collected. Two-dimensional ^{1}H-^{1}H nuclear Overhauser effect spectroscopy (NOESY) data were collected for the MG-aptamer RNA alone, and RNA was mixed with equimolar of MG and 4 mg/mL montmorillonite. To improve the spectral quality, the montmorillonite-containing sample was centrifuged at 12,000 rpm for 1 min to remove the insoluble mineral. All the NMR data were collected in D_2O (99.96%; CIL, Tewksbury, MA) at 308 K on a Bruker Avance III 800 MHz spectrometer equipped with TCI cryoprobe (NMR Core, University of Missouri). The NMR data were processed by NMRPipe (63) and analyzed by NMRViewJ (64).

RESULTS

Binding of the MG aptamer to montmorillonite

Binding of the MG-aptamer RNA to montmorillonite in the absence of MG was measured using fluorescent labeling of the 5′ end of the RNA with a maleimide derivative of Alexa Fluor 647 (Thermo Fisher). The labeled RNA was mixed with a variable amount of montmorillonite. The mixture was incubated overnight for equilibration (Fig. S1 *a*) and separated by centrifugation. The fraction of bound RNA (f_b) was calculated from the supernatant fluorescence (F_{sup}) (unbound RNA) compared to the total RNA fluorescence F_0 (measured before addition of montmorillonite) ($f_b = 1 - F_{sup}/F_0$). The fraction of bound RNA increased with montmorillonite concentration and could be fit to a ligand-receptor model (Hill coefficient = 1; or equivalently, the Langmuir isotherm model for adsorption), yielding an apparent association constant (K_a) value of 0.11 ± 0.05 mL/mg (apparent dissociation constant $K_D = 1/K_a$ = 9.1 mg/mL, i.e., half-maximal RNA bound at 9.1 mg/mL montmorillonite) (Fig. 1). At [montmorillonite] = apparent K_D, the mass equivalent of an approximately 0.06 μM RNA solution was bound, corresponding to a density of roughly 7 nmol of RNA bound per gram of montmorillonite.

Desorption and equilibration with montmorillonite were observed by measuring the amount of fluorescently labeled RNA aptamer released into free solution over 4 days. The amount of RNA in solution remained around 4%–8% over time (Fig. S1 *b*). The saturable binding (Fig. S1 *a*) and little change in amount of free RNA suggest equilibration of the mixture.

Decreased fluorescence of the MG aptamer in the presence of montmorillonite

Binding of MG by the aptamer restricts the vibrational deexcitation of MG, resulting in a ∼2360-fold increase in fluorescence (57). Aptamer binding activity can thus be monitored by MG fluorescence (43,57). We measured the fluorescence of the MG-aptamer complex at different concentrations of montmorillonite (Fig. 2), with a near-saturating amount of MG ([RNA] = 0.2 μM, [MG] = 12 μM, given an apparent K_D of 2.5 μM for the MG-aptamer complex in aqueous buffer (52)). The apparent K_D of the MG-aptamer complex was also determined in the presence of buffer that was preincubated with montmorillonite and then centrifuged to remove montmorillonite, giving a value of 2.4 ± 0.4 μM (Fig. S2 *a*), indicating that solutes potentially leaching from montmorillonite did not cause a change in MG-aptamer K_D. The fluorescence of the MG-aptamer complex decreased with increasing montmorillonite (Fig. 2), suggesting that montmorillonite interfered with binding between the aptamer and MG. However, this trend was observed at concentrations of montmorillonite well

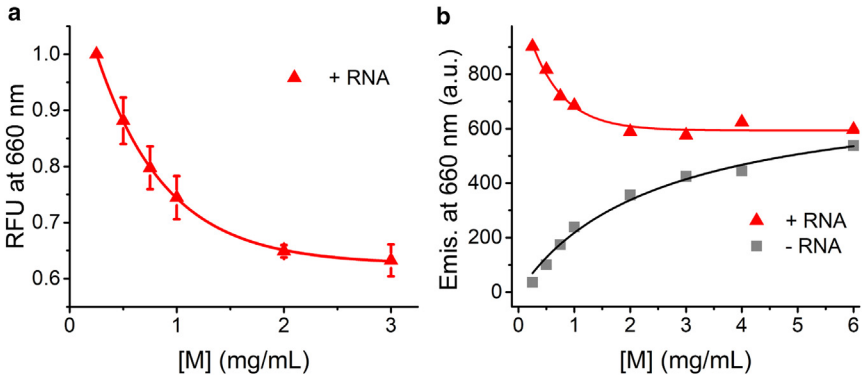

FIGURE 2 MG fluorescence in the presence of montmorillonite. Fluorescence of the bulk MG-aptamer solution decreased with increased montmorillonite concentration (*red curve*; normalized to 1 at [montmorillonite] = 0.25 mg/mL in *a*; unnormalized in *b*). In contrast, MG fluorescence of the control solution without aptamer (*gray*) increases with increasing montmorillonite (*b*; one representative series is shown). Curve shown in (*a*) was fit to $F = 0.55 \times \exp(-M/0.65) + 0.63$, where F is fluorescence and M is [montmorillonite]; red curve in (*b*) was fit to $F = 593 + 487 \times \exp(-M/0.58)$, to guide the eye; gray curve was fit to isotherm $F = 757M/(2.48 + M)$. RFU, relative fluorescence units; a.u., arbitrary units. Fluorescence was measured by excitation at 617 nm and emission at 660 nm. Error bars in *a* represent standard deviation of three independent experiments ($N = 3$).

below the apparent K_D of the montmorillonite-aptamer binding equilibrium (Fig. 1; measured in the absence of MG), so the decreasing fluorescence (in the presence of MG) could not be explained only by reduced MG binding by montmorillonite-bound aptamer. We hypothesized that relatively low concentrations of montmorillonite may bind directly to MG and thus reduce fluorescence of the ternary aptamer-MG-montmorillonite system.

To determine whether montmorillonite had the potential to bind MG in competition with aptamer, MG was also added to increasing concentrations of montmorillonite in the absence of aptamer. Without aptamer, MG fluorescence increased with increasing concentration of montmorillonite (Fig. 2 *b* (*gray*), Fig. S2 *b*), indicating that MG can bind directly to montmorillonite. Therefore, in the presence of [montmorillonite], MG may bind to the aptamer or to montmorillonite itself.

While the observed MG fluorescence increase without aptamer indicated that the turbidity caused by the montmorillonite suspension was relatively limited, nevertheless a technique that did not rely on absolute fluorescence was preferable to avoid potential confounding by turbidity effects. Thus, to study the possible change in binding of MG, we measured the emission spectrum of MG when bound to the aptamer or when bound to montmorillonite (Fig. 3 *a*, black vs. green line). The peak position was red-shifted by >20 nm when bound to montmorillonite compared to the MG-aptamer complex, so the peak position could be used to discriminate between montmorillonite-bound MG and aptamer-bound MG. In the ternary system, addition of montmorillonite to the MG-aptamer solution led to gradual red shifting, with the emission spectrum at higher [montmorillonite] resembling the spectrum of MG bound to montmorillonite in the absence of aptamer (Fig. 3 *a*). The spectral change indicates a change in the local environment of MG, from aptamer-bound to montmorillonite-bound, as the montmorillonite concentration increased. Interestingly, the concentration of montmorillonite resulting in half-maximal peak shift (0.6 mg/mL; Fig. 3 *b*) was more than an order of magnitude lower than the apparent K_D of aptamer-montmorillonite adsorption (9.1 mg/mL; Fig. 1), indicating that MG release from the aptamer and uptake by the mineral occurs at ~10-fold lower [montmorillonite] compared to RNA binding to montmorillonite.

Effect of montmorillonite on the aptamer-dye interaction monitored by FRET

To confirm the release of MG by the aptamer in the presence of relatively low concentrations of montmorillonite (below the apparent K_D of the aptamer-montmorillonite interaction), we employed FRET between a 5′ donor label (fluorescein; emission at ~520 nm) and the MG dye itself as acceptor (emission at ~655 nm). Presence of an FRET signal would depend on MG dye being bound and in proximity to the 5′ donor label (Fig. 4 *a*). When a saturating concentration of MG was added to the aptamer, donor emission intensity decreased while a new peak at the acceptor wavelength was observed, consistent with FRET (Fig. 4 *b*; FRET efficiency $E = 22.3\% \pm 1.5\%$, based on the decrease of donor intensity). The FRET signal was decreased upon thermal melting of the aptamer, as expected, confirming the use of FRET to monitor proximity in this context (Fig. S3). When montmorillonite (1 mg/mL) was present, addition of MG showed reduced FRET with no detectable acceptor signal (Fig. 4 *c*) ($E = 15\% \pm 1\%$), indicating RNA denaturation and/or dissociation of the dye.

Melting transition of the MG aptamer in the presence of montmorillonite

The observation that low concentrations (e.g., 1 mg/mL) of montmorillonite caused aptamer-dye dissociation, without substantial RNA binding to montmorillonite that was stable to washing, raised the intriguing possibility that montmorillonite may have a denaturing effect on RNA folding, even when not tightly bound to RNA. To characterize aptamer

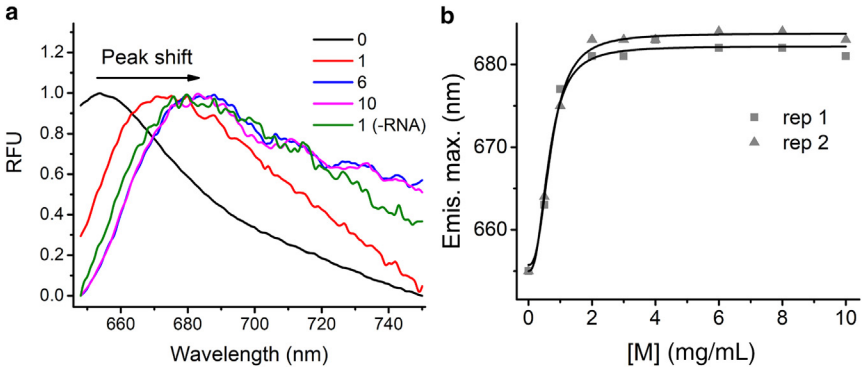

FIGURE 3 Emission spectra of MG with aptamer and montmorillonite. (*a*) Steady-state emission spectra of MG with aptamer in 0 (*black*), 1 (*red*), 6 (*blue*), or 10 (*magenta*) mg/mL concentrations of montmorillonite (see legend, *inset*). The emission peak at 10 mg/mL montmorillonite (*magenta*) is similar to the aptamer-free solution with 1 mg/mL montmorillonite (*green*). [MG] = 12 μM, [aptamer] = 0.2 μM. (*b*) Change in peak wavelength of emission, plotted against montmorillonite concentration, fitted by the Hill equation (apparent K_D = 0.61 (n = 2.50) and 0.64 mg/mL (n = 2.56) for replicates 1 and 2, respectively; n = Hill coefficient). RFU, relative fluorescence units. Fluorescence was measured by excitation at 617 nm.

stability at a relatively low concentration of montmorillonite (below the aptamer-montmorillonite apparent K_D of 9.1 mg/mL), the melting curve of the aptamer-MG complex was measured at 1 mg/mL montmorillonite. At this low [montmorillonite], a measurable fraction of the MG-aptamer complex appeared to be intact at room temperature (Fig. 2). The melting transition of the MG-aptamer complex was monitored by fluorescence of MG, which reports on structural changes affecting MG binding (e.g., changes in the ligand-binding site) (43,52). The transition temperature (T_t) of the MG-aptamer complex was 34.2°C ± 2.3°C in mineral-free solution, but decreased to 15.8°C ± 1.3°C in the presence of 1 mg/mL montmorillonite (Fig. 6 *a*), indicating that the aptamer-MG interaction was destabilized in the presence of 1 mg/mL montmorillonite. The melting curve was similar when repeated again with the same sample, indicating an equilibrium measurement (Fig. S4 *a*). The fluorescence of MG itself bound to montmorillonite (without aptamer) was insensitive to temperature changes in the same range (Fig. S4 *b*). Thus, while multiple observations described above (reduction of MG-aptamer fluorescence intensity, the fluorescence peak shift, and FRET reduction), made at relatively low montmorillonite concentrations, indicated that MG was released from the aptamer and bound to the mineral, it had not been clear whether these observations were due only to competitive binding or whether the presence of montmorillonite might additionally destabilize the aptamer-dye interaction to facilitate release. The observed change in the melting transition indicated that the MG-aptamer interaction was indeed perturbed by the presence of montmorillonite (1 mg/mL).

MG-aptamer contacts analyzed by NMR

The structure of the MG aptamer consists of two stems, an internal GAGA stem-loop and a stem formed from annealing of the 3′ and 5′ terminal regions, which bracket either side of the binding pocket (62). In the absence of montmorillonite, the MG-bound aptamer RNA exhibited sharp and dispersed peaks in the 1D ^{1}H spectrum (Fig. 5 *a*), indicating that the RNA folded into a stable structure. Addition of 0.4–4 mg/mL montmorillonite resulted in substantial broadening of peaks, suggesting possible denaturation of the MG-aptamer RNA upon montmorillonite titration. To characterize the structural changes of MG aptamer induced by montmorillonite, 2D ^{1}H-^{1}H NOESY data were collected. Resonance assignment of aromatic protons in the MG-aptamer-identified NOE patterns that support the formation of the terminal stem (G1-C5: G34-C38) and internal stem (U11-C14: G19-A22) with a GAGA tetraloop, consistent with previous NMR studies of the MG aptamer (Fig. 5, *b* and *c*) (62). In the presence of a moderate concentration of montmorillonite (4 mg/mL), the signals corresponding to the terminal stem and the bulge of the binding pocket were undetectable or substantially broadened, while signals corresponding to the internal stem and GAGA tetraloop remained intact (Fig. 5 *b*). These results indicate that 4 mg/mL montmorillonite denatured the terminal stem and the bulge to abolish MG binding, while the GAGA-containing stem-loop remained unaffected (Fig. 5 *c*).

Adsorption and melting of an RNA duplex on montmorillonite

As seen for the RNA aptamer, a fluorescently labeled single-strand RNA (ssRNA) oligonucleotide (10 bases in length) adsorbed strongly to the montmorillonite surface (Fig. S5). Interestingly, the apparent K_a value of 11.1 ± 2.3 mL/mg (apparent K_D = 0.09 mg/mL), determined from the binding curve, was ∼100-fold higher than the apparent K_a observed for the RNA aptamer (Fig. 1 and Table 1), indicating substantially stronger binding of the oligonucleotide to montmorillonite.

Given that the data from the MG aptamer indicated destabilization of the binding pocket in the presence of montmorillonite, we tested whether the secondary structure of an RNA duplex would also be destabilized when adsorbed onto montmorillonite. Although light scattering from the mineral particles interferes with monitoring of secondary structure by circular dichroism, FRET can be used to probe

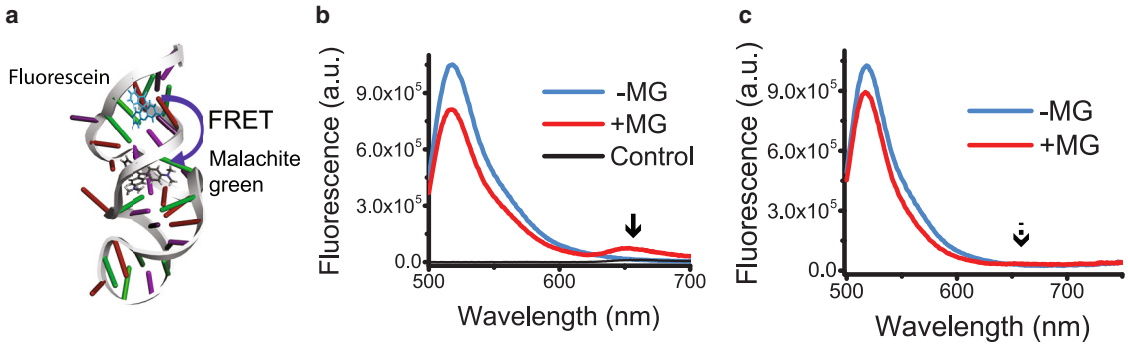

FIGURE 4 FRET between fluorescein label at the 5′ end of the MG aptamer (donor) and the MG dye (acceptor). (*a*) Schematic representation of the FRET between the 5′-fluorescein label and MG present at the binding pocket of the aptamer. (*b*) In the absence of montmorillonite, no acceptor signal was observed without MG (*blue*), but an FRET signal (indicated by an *arrow*) was observed when MG was added (*red*). Control (*black*) = MG dye alone. (*c*) In the presence of 1 mg/mL montmorillonite, the acceptor signal was not detectable. [MG] = 23.6 μM, [aptamer] = 1.05 μM. a.u., arbitrary units. Fluorescence emission spectra were measured with excitation at 480 nm.

duplex formation of a doubly labeled RNA duplex (Fig. 6 *b*). The melting temperature (T_m) of the RNA oligonucleotide, annealed as a duplex with a complementary RNA oligonucleotide, was determined by monitoring the ratio of donor-to-acceptor fluorescence with increasing temperature. In solution without montmorillonite, the T_m of the preannealed duplex was found to be 24.3°C ± 2.3°C, and with montmorillonite (10 mg/mL) the T_m was not significantly changed (22.8°C ± 1.2°C; Table 2 and Fig. 6 *c*). Therefore, in contrast to the aptamer binding pocket, adsorption to montmorillonite did not appear to destabilize the RNA duplex significantly. Adsorption to montmorillonite was confirmed by incubating the RNA duplex with montmorillonite and checking for depletion of both strands from the supernatant, at both room temperature and 37°C (Fig. S6). To determine whether the RNA duplex could also become hybridized in the presence of montmorillonite, we first adsorbed one RNA strand to montmorillonite and then added the second strand. The resulting RNA exhibited a similar melting temperature (25°C; Fig. 6 *c*), indicating that ssRNA adsorbed to montmorillonite was capable of hybridizing with its complementary strand.

Adsorption and melting of DNA on montmorillonite

To probe the generality of nucleic acid adsorption onto montmorillonite, we also studied how montmorillonite affected a DNA duplex and a DNA hairpin using FRET (Fig. 7, *a* and *b*). These structures are analogous to each other, sharing the same base pairs, except that the DNA hairpin includes a poly(T) tetraloop. The apparent K_a values were estimated to be 0.32 ± 0.02 mL/mg (apparent K_D = 3.13 mg/mL) for an ssDNA oligonucleotide and 0.032 ± 0.005 mL/mg (apparent K_D = 31.3 mg/mL) for the DNA hairpin in the presence of Mg-citrate (Figs. S7 and S8; Table 1). The ssDNA apparently bound more weakly than the ssRNA oligonucleotide to montmorillonite, and the DNA hairpin bound more weakly than both single-stranded oligonucleotides or the aptamer to montmorillonite. However, binding of both DNAs was greater in the presence of $MgCl_2$ compared to Mg-citrate (Figs. S7 and S8; Table 1). As observed for the RNA duplex, the melting temperatures of both the DNA duplex and the DNA hairpin were not significantly perturbed by binding to montmorillonite (10 mg/mL) (Table 2), although the shapes of the melting curves were somewhat altered (Fig. 7, *a* and *b*), suggesting possible changes in the cooperativity of the melting transitions. Adsorption to montmorillonite was confirmed by incubating the DNA duplex with montmorillonite and checking for depletion of both strands from the supernatant, at both room temperature and 37°C (Fig. S6).

DISCUSSION

The predicted presence and possible importance of minerals during early prebiotic evolution creates a need to understand how minerals affect RNA folding and function. The known adsorption of nucleic acids to minerals raises the possibility that folding and, thus, function could be substantially perturbed by minerals, an expectation that has been supported by simulation studies. While self-cleaving ribozymes were found to be relatively tolerant of montmorillonite (48), molecular dynamics studies suggested that the reason for this is that the mineral promotes an alternative catalytic mechanism for the ribozyme, a feature that might not be available more generally to functional RNAs (51). Here we expanded the scope of experimental work to understand the effect of montmorillonite on nucleic acids, including both secondary and tertiary structure, by studying the MG aptamer, an ssRNA oligonucleotide, an RNA duplex, a DNA duplex, and a DNA hairpin.

Adsorption of each nucleic acid to montmorillonite could be fit to a Langmuir adsorption isotherm model, yielding an apparent association constant K_a. Certain mineral surfaces have been shown to selectively enrich longer RNA

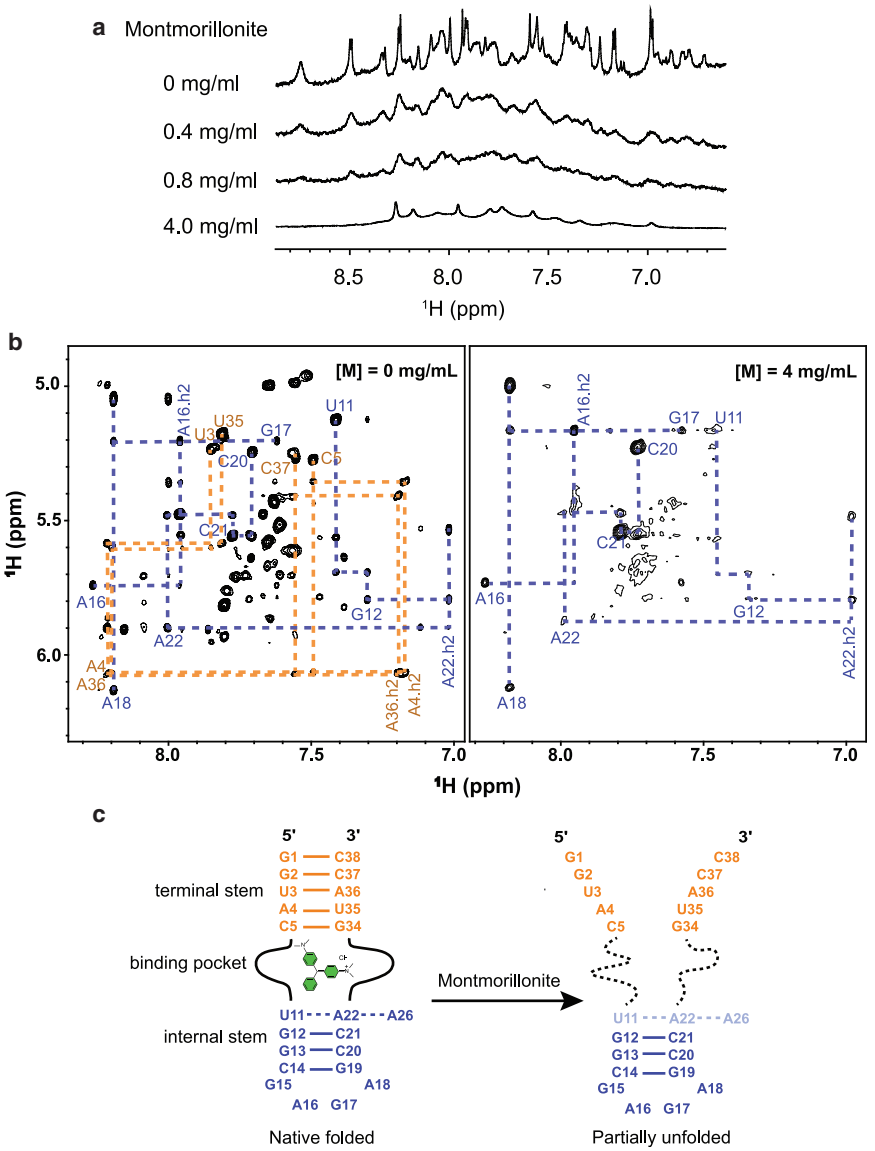

FIGURE 5 Structural changes in the MG aptamer probed by NMR. (*a*) The aromatic proton region of 1D NMR spectra collected for MG aptamer upon montmorillonite titration is shown. (*b*) Aromatic region of 2D NOESY NMR spectra in the absence (*left*) or presence (*right*) of montmorillonite (4 mg/mL) are shown. The NOE connectivities between ribose H1′ proton and aromatic H8/H6 proton in the internal stem and the terminal stem are denoted as blue and orange dashed lines, respectively. H2 protons of adenosines (A4, A22, and A36) are labeled vertically (denoted as ".h2"). NMR signals from the terminal stem broadened or disappeared in the presence of montmorillonite, suggesting the base pairings were no longer formed. The signal intensity of U11 and A22 are weaker than the intensities without montmorillonite, indicating partial denaturation of U11-A22-A26 base interactions (indicated by *lighter color*). (*c*) Schematic representation of the secondary structure of MG aptamer in presence and absence of 4 mg/mL montmorillonite.

molecules due to the free energy penalty for covering the same surface with smaller oligomers (18). For example, the *Azoarcus* recombinase ribozyme can self-assemble to produce multiple products, the longest of which (300–350 nt) could be accumulated on mineral surfaces (18). If adsorbed RNAs were functional, this effect could provide a chemical selection for increasing the information content of the adsorbed RNAs. However, here we observed that although ssRNA (10 nt) bound strongly to montmorillonite, the binding affinities of ssDNA and the structured nucleic acids, namely the DNA hairpin (24 nt) and the MG RNA aptamer (38 nt), to montmorillonite were relatively weak, despite being longer sequences. The relative weakness of structured nucleic acids binding to montmorillonite might be understood to be due to electrostatic considerations. Cations are required to mediate the interaction between the negatively charged mineral surface and the negatively charged phosphate backbone of the nucleic acids (65). For example, in one study, divalent Ca^{+2}- or Mg^{+2}-montmorillonite was more effective for adsorption of polyadenylic acid, polyuridylic acid, polydeoxyadenylic acid, polydeoxythymidylic acid, and chromosomal DNA compared to monovalent Na^{+}-montmorillonite (23). Montmorillonite K10, used in the present study, is a commercially available acid-treated preparation containing a mixture of cations including K^{+}, Na^{+}, and Ca^{2+}. While the acid treatment is expected to replace exchangeable cations by protons (66–68), buffers used in these experiments also contained monovalent and divalent cations, and the pH change associated with montmorillonite addition was relatively small (<0.1 pH unit change given up to 20 mg/mL montmorillonite K10; Table S2). Due to its pretreatment, montmorillonite

TABLE 1 K_a values of binding with montmorillonite

Sample	Apparent K_a for montmorillonite (mL/mg)	Apparent K_D ($1/K_a$) for montmorillonite (mg/mL)
MG aptamer	0.11 ± 0.05	9.1
ssRNA (TAMRA-labeled)	11.1 ± 2.3	0.09
ssDNA (TAMRA-labeled)	0.32 ± 0.02 (Mg-citrate)	3.13
ssDNA (fluorescein-labeled)	1.22 ± 0.15 ($MgCl_2$)	0.82
DNA hairpin	0.032 ± 0.005 (Mg-citrate)	31.3
	0.32 ± 0.04 ($MgCl_2$)	3.13
MG	0.35 ± 0.10	2.86

Results from direct nonlinear fitting to the binding curve are given for all entries except MG (Fig. S2 *b*).

K10 lacks interlayer channels of smectite clays, which may inhibit the ability to catalyze RNA polymerization (26,40,69), and does not occur naturally. While adjustment of the montmorillonite preparation and salt and buffer conditions would likely influence its binding properties, the comparisons among different nucleic acids in the present study pertain to the same clay preparation and solution conditions. Double-stranded nucleic acids, having increased negative charge per molecular length unit compared to single-stranded nucleic acids, are known to be less well adsorbed (23), consistent with the pattern of apparent K_a values observed here. This difference might be mitigated by higher cation concentrations resulting in greater charge shielding. In addition to electrostatic interactions, hydrogen bonding and van der Waals forces can contribute to adsorption of nucleic acids to montmorillonite (17,26), possibly contributing to the difference noted between ssRNA and ssDNA. For large DNAs, structural configuration also plays an important role, as closed circular plasmid DNA adsorbs more poorly than linear double-stranded DNA due to the difference in accessibility of interacting groups (70). Although the experiments reported here were not designed to study the mechanism of nucleic acid binding to montmorillonite, ssDNA and ssRNA adsorbed to montmorillonite were found to be capable of forming a stable duplex with the complementary strand, consistent with earlier reports (47), and the melting temperature of the adsorbed DNA hairpin was not affected by adsorption to montmorillonite. These observations indicate that secondary structures may still form and remain intact on montmorillonite, consistent with the retention of certain ribozyme activities, at least at a low level, and templating ability (as described above). Thus, although adsorption of structured nucleic acids is relatively weak compared to single strands, some secondary structures appear to be relatively unperturbed on montmorillonite.

At the same time, certain secondary and tertiary structures and, thus, function were sensitive to adsorption. The MG aptamer is an RNA consisting of a ligand-binding loop between two helical regions. The ligand-binding site includes base pairs, a base triple, and a base quadruple, as well as orthogonal interactions between bases and the ligand (71). Binding of the ligand relies primarily on stacking and electrostatic interactions and includes an entropic penalty due to restriction of the MG ligand (72). Although MG binding does not require Mg^{2+} (71), the binding pocket is stabilized by monovalent or divalent metal ions, permitting a contrast to the case of the hammerhead ribozyme, where

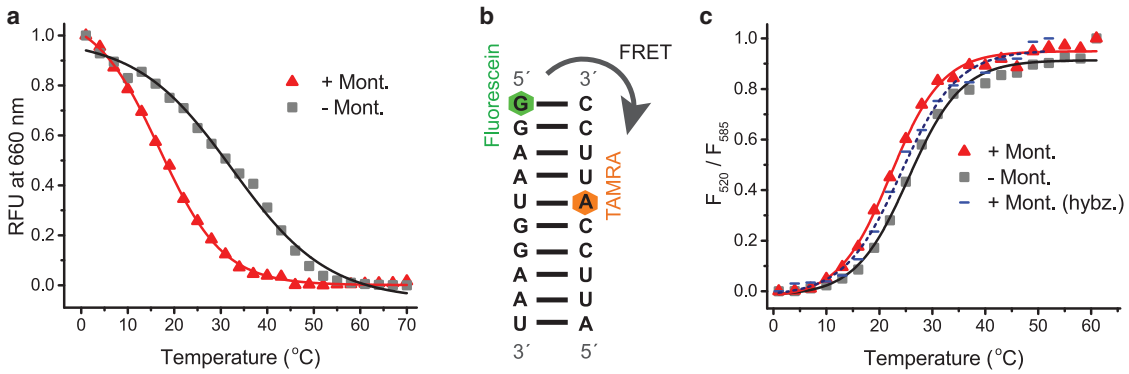

FIGURE 6 Melting studies with RNA and montmorillonite. (*a*) Bulk fluorescence of the MG aptamer was monitored in the presence (*red triangles*) or absence (*gray squares*) of 1 mg/mL montmorillonite at various temperatures. A representative plot is shown; data were obtained for three independent samples. Fluorescence was normalized to the value at 1°C (excitation at 617 nm, emission at 660 nm). RFU, relative fluorescence units. (T_m = 15.8°C ± 1.3°C with montmorillonite and 34.2°C ± 2.3°C without montmorillonite.) (*b*) Schematic representation of the 10-bp RNA duplex with FRET labels. (*c*) Melting curves of the RNA duplex, formed through stepwise addition of the two strands (*dotted line*), with (*red triangles*) or without (*gray squares*) 10 mg/mL montmorillonite. Fluorescence was measured with excitation at 450 nm and emission at 520 and 585 nm. The ratio F_{520}/F_{585} was normalized between 0 and 1. (T_m = 22.8°C ± 1.2°C with montmorillonite and 24.3°C ± 2.3°C without montmorillonite.).

TABLE 2 Melting temperatures of oligonucleotides adsorbed on montmorillonite

Sample	Buffer only	Montmorillonite (10 mg/mL)
RNA duplex	24.3°C ± 2.3°C	22.8°C ± 1.2°C
DNA duplex	10.5°C ± 0.6°C	9.8°C ± 0.2°C
DNA hairpin	68.4°C ± 1.9°C	69.1°C ± 2.5°C

simulations indicated that the loss of Mg^{2+} upon binding to clay could be compensated by adoption of a new Mg^{2+}-independent mechanism (51). Here, multiple observations (decreased fluorescence, red-shifted emission spectrum, decreased FRET, lower melting transition temperature) indicated a loss of MG-aptamer binding in the presence of montmorillonite. In addition, 2D NOESY NMR spectra collected in the presence and absence of montmorillonite showed that while the GAGA stem-loop was intact in the presence of montmorillonite, the terminal stem and bulge residues of the binding pocket were denatured. Given that the terminal stem anchors one end of the binding pocket, this structural disruption is the likely cause of decreased aptamer activity. Prior studies suggest that the terminal base could tether the RNA to the montmorillonite (24), in addition to electrostatic interactions with the mineral that can cause conformational changes in ssRNA (65). Thus, interaction of the RNA terminus with montmorillonite appears to lead to denaturation of the terminal stem, disrupting binding activity, although the GAGA tetraloop hairpin was relatively unperturbed. Interestingly, the GAGA tetraloop belongs to the GNRA tetraloop (N = A, U, G, C; R = A, G) family known to lower the Gibbs free energy of the internal stem, forming an unusually stable structure that includes a G-A wobble pair, additional H-bonds, and extensive base stacking (73–75), perhaps enabling its preservation in the presence of montmorillonite.

These results suggest that while some processes involving duplexes, such as hairpin formation and templating for replication, may tolerate adsorption of the RNA to montmorillonite, functional RNAs may or may not be compatible with adsorption depending on whether binding to montmorillonite disrupts functionally important contacts. Whether an aptamer or ribozyme retains activity would depend on details of its mechanism and on the specifics of its interactions with the surface as well as dissolved salts and solution conditions. While self-cleaving ribozymes have been shown to tolerate adsorption with only moderate loss of activity, this tolerance is not generalizable, as the present studies using the MG aptamer demonstrate. If montmorillonite, or other clay minerals, were the site of the RNA world, the surface itself would be a limiting factor in determining which activities and mechanisms could emerge.

SUPPORTING MATERIAL

Supporting material can be found online at https://doi.org/10.1016/j.bpj.2023.11.002.

AUTHOR CONTRIBUTIONS

R.S., X.H., and I.A.C. designed research. R.S., W.-L.K., and B.M. performed research. R.S. analyzed data. W.-L.K. and X.H. analyzed NMR data. R.S., W.-L.K., X.H., and I.A.C. wrote the manuscript.

ACKNOWLEDGMENTS

Technical assistance was provided by Krishna Burton. Funding was provided by the Simons Foundation Collaboration on the Origin of Life (290356FY18), NASA (80NSSC21K0595, 80NSSC21K0596), NSF (2318736), Sloan Foundation (AWD103574), Moore Foundation (AWD103653), and the Camille Dreyfus Teacher-Scholar Program.

DECLARATION OF INTERESTS

The authors declare no competing interests.

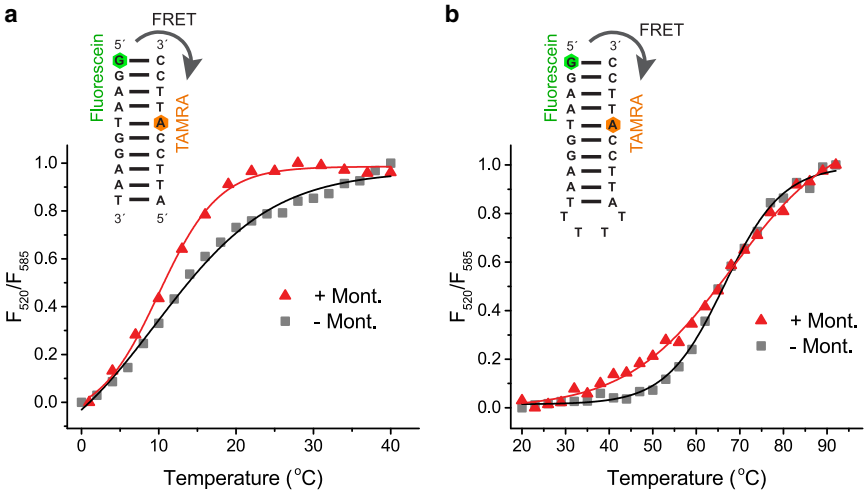

FIGURE 7 Melting of DNA constructs with montmorillonite. Melting curves for the DNA duplex (*a*) and DNA hairpin (*b*) with (*red triangles*) or without (*gray squares*) 10 mg/mL montmorillonite show little effect of montmorillonite on melting temperature. Schematic diagrams of the DNA constructs are shown with FRET labels in respective insets. Fluorescence was measured with excitation at 450 nm and emission at 520 and 585 nm. The ratio F_{520}/F_{585} was normalized between 0 and 1. (T_m for DNA duplex: 9.8°C ± 0.2°C with montmorillonite, 10.5°C ± 0.6°C without montmorillonite; T_m for hairpin: 69.1°C ± 2.5°C with montmorillonite, 68.4°C ± 1.9°C without montmorillonite).

REFERENCES

1. Kruger, K., P. J. Grabowski, …, T. R. Cech. 1982. Self-splicing RNA: Autoexcision and autocyclization of the ribosomal RNA intervening sequence of tetrahymena. *Cell.* 31:147–157.
2. Guerrier-Takada, C., K. Gardiner, …, S. Altman. 1983. The RNA moiety of ribonuclease P is the catalytic subunit of the enzyme. *Cell.* 35:849–857.
3. The "Strong" RNA World Hypothesis, Kim, H. J., and S. A. Benner 2013. Fifty Years Old. *Astrobiology.* 13:391–403.
4. Orgel, L. E. 1986. RNA catalysis and the origins of life. *J. Theor. Biol.* 123:127–149.
5. Woese, C. R. 1967. The Genetic Code: The Molecular Basis for Genetic Expression. Harper and Row.
6. Crick, F. H. C. 1968. The origin of the genetic code. *J. Mol. Biol.* 38:367–379.
7. Orgel, L. E. 1968. Evolution of the genetic apparatus. *J. Mol. Biol.* 38:381–393.
8. Powner, M. W., B. Gerland, and J. D. Sutherland. 2009. Synthesis of activated pyrimidine ribonucleotides in prebiotically plausible conditions. *Nature.* 459:239–242.
9. Powner, M., J. Sutherland, and J. Szostak. 2011. The origins of nucleotides. *Synlett.* 2011:1956–1964.
10. Walton, T., W. Zhang, …, J. W. Szostak. 2019. The mechanism of nonenzymatic template copying with imidazole-activated nucleotides. *Angew. Chem. Int. Ed.* 58:10812–10819.
11. Joyce, G. F., T. Inoue, and L. E. Orgel. 1984. Non-enzymatic template-directed synthesis on RNA random copolymers: Poly(C, U) templates. *J. Mol. Biol.* 176:279–306.
12. Ellington, A. D., and J. W. Szostak. 1990. In vitro selection of RNA molecules that bind specific ligands. *Nature.* 346:818–822.
13. Leveau, G., D. Pfeffer, …, C. Richert. 2022. Enzyme-free copying of 12 bases of RNA with dinucleotides. *Angew. Chem. Int. Ed.* 61, e202203067.
14. Le Vay, K., E. Salibi, …, H. Mutschler. 2020. Nucleic acid catalysis under potential prebiotic conditions. *Chem. Asian J.* 15:214–230.
15. Szabó, P., I. Scheuring, …, E. Szathmáry. 2002. In silico simulations reveal that replicators with limited dispersal evolve towards higher efficiency and fidelity. *Nature.* 420:340–343.
16. Bansho, Y., T. Furubayashi, …, T. Yomo. 2016. Host–parasite oscillation dynamics and evolution in a compartmentalized RNA replication system. *Proc. Natl. Acad. Sci. USA.* 113:4045–4050.
17. Hashizume, H. 2015. Adsorption of nucleic acid bases, ribose, and phosphate by some clay minerals. *Life.* 5:637–650.
18. Mizuuchi, R., A. Blokhuis, …, D. Baum. 2019. Mineral surfaces select for longer RNA molecules. *Chem. Commun.* 55:2090–2093.
19. Pedreira-Segade, U., J. Hao, …, I. Daniel. 2018. How do nucleotides adsorb onto clays? *Life.* 8, 59.
20. Feuillie, C., I. Daniel, …, U. Pedreira-Segade. 2013. Adsorption of nucleotides onto Fe-Mg-Al rich swelling clays. *Geochem. Cosmochim. Acta.* 120:97–108.
21. Kaddour, H., S. Gerislioglu, …, N. Sahai. 2018. Nonenzymatic RNA oligomerization at the mineral-water interface: an insight into the adsorption-polymerization relationship. *J. Phys. Chem. C.* 122:29386–29397.
22. Kevadiya, B. D., and H. C. Bajaj. 2013. The layered silicate, montmorillonite (MMT) as a drug delivery carrier. *Key Eng. Mater.* 571:111–132.
23. Franchi, M., J. P. Ferris, and E. Gallori. 2003. Cations as mediators of the adsorption of nucleic acids on clay surfaces in prebiotic environments. *Orig. Life Evol. Biosph.* 33:1–16.
24. Swadling, J. B., P. V. Coveney, and H. C. Greenwell. 2010. Clay minerals mediate folding and regioselective interactions of RNA: a large-scale atomistic simulation study. *J. Am. Chem. Soc.* 132:13750–13764.
25. Villafañe-Barajas, S. A., J. P. T. Baú, …, D. A. M. Zaia. 2018. Salinity effects on the adsorption of nucleic acid compounds on Na-montmorillonite: a prebiotic chemistry experiment. *Orig. Life Evol. Biosph.* 48:181–200.
26. Yu, W. H., N. Li, …, C. Y. Xu. 2013. Adsorption of proteins and nucleic acids on clay minerals and their interactions: A review. *Appl. Clay Sci.* 80–81:443–452.
27. Biondi, E., Y. Furukawa, …, S. A. Benner. 2017. Adsorption of RNA on mineral surfaces and mineral precipitates. *Beilstein J. Org. Chem.* 13:393–404.
28. Hazen, R. M., D. A. Sverjensky, …, R. E. Milliken. 2013. Clay mineral evolution. *Am. Mineral.* 98:2007–2029.
29. Bristow, T. F., and R. E. Milliken. 2011. Terrestrial perspective on authigenic clay mineral production in ancient Martian lakes. *Clay Clay Miner.* 59:339–358.
30. Hanczyc, M. M., S. S. Mansy, and J. W. Szostak. 2007. Mineral surface directed membrane assembly. *Orig. Life Evol. Biosph.* 37:67–82.
31. Dalai, P., and N. Sahai. 2020. A model protometabolic pathway across protocell membranes assisted by photocatalytic minerals. *J. Phys. Chem. C.* 124:1469–1477.
32. Bernal, J. D. 1949. The physical basis of life. *Proc. Phys. Soc.* 62:537–558.
33. Cleaves, H. J., 2nd, A. Michalkova Scott, …, R. Hazen. 2012. Mineral–organic interfacial processes: potential roles in the origins of life. *Chem. Soc. Rev.* 41:5502–5525.
34. Hazen, R. M., and D. A. Sverjensky. 2010. Mineral surfaces, geochemical complexities, and the origins of life. *Cold Spring Harbor Perspect. Biol.* 2, a002162.
35. Erastova, V., M. T. Degiacomi, …, H. C. Greenwell. 2017. Mineral surface chemistry control for origin of prebiotic peptides. *Nat. Commun.* 8:2033.
36. Ferris, J. P., A. R. Hill, …, L. E. Orgel. 1996. Synthesis of long prebiotic oligomers on mineral surfaces. *Nature.* 381:59–61.
37. Ferris, J. P. 2002. Montmorillonite catalysis of 30–50 mer oligonucleotides: laboratory demonstration of potential steps in the origin of the RNA World. *Orig. Life Evol. Biosph.* 32:311–332.
38. Huang, W., and J. P. Ferris. 2006. One-step, regioselective synthesis of up to 50-mers of RNA oligomers by montmorillonite catalysis. *J. Am. Chem. Soc.* 128:8914–8919.
39. Joshi, P. C., M. F. Aldersley, …, J. P. Ferris. 2009. Mechanism of montmorillonite catalysis in the formation of RNA oligomers. *J. Am. Chem. Soc.* 131:13369–13374.
40. Aldersley, M. F., P. C. Joshi, …, J. P. Ferris. 2011. The role of montmorillonite in its catalysis of RNA synthesis. *Appl. Clay Sci.* 54:1–14.
41. Namani, T., S. Snyder, …, N. Sahai. 2021. Amino acid specific nonenzymatic montmorillonite-promoted RNA polymerization. *ChemSystemsChem.* 3, e2000060.
42. Šponer, J. E., J. Šponer, …, A. Kovařík. 2021. Nonenzymatic, template-free polymerization of 3',5' cyclic guanosine monophosphate on mineral surfaces. *ChemSystemsChem.* 3, e2100017.
43. Saha, R., and I. A. Chen. 2019. Effect of UV radiation on fluorescent RNA aptamers' functional and templating Ability. *Chembiochem.* 20:2609–2617.
44. Singer, B. 1971. Chemical modification of viral ribonucleic acid: IX. The effect of ultraviolet irradiation on TMV-RNA and other polynucleotides. *Virology.* 45:101–107.
45. Aguilar-Ovando, E., and A. Negron-Mendoza. 2010. Radiation chemistry approach to the study of sedimentary microenvironments as models for the protection of bio-organic molecules on the early earth. *J. Radioanal. Nucl. Chem.* 286:637–642.
46. Biondi, E., S. Branciamore, …, E. Gallori. 2007. Montmorillonite protection of an UV-irradiated hairpin ribozyme: evolution of the RNA world in a mineral environment. *BMC Evol. Biol.* 7 (*Suppl 2*):S2.

47. Franchi, M., and E. Gallori. 2005. A surface-mediated origin of the RNA world: biogenic activities of clay-adsorbed RNA molecules. *Gene.* 346:205–214.
48. Biondi, E., S. Branciamore, …, E. Gallori. 2007. Catalytic activity of hammerhead ribozymes in a clay mineral environment: Implications for the RNA world. *Gene.* 389:10–18.
49. Kawamura, K., J. F. Lambert, …, M. C. Maurel. 2022. Life on minerals: binding behaviors of oligonucleotides on zirconium silicate and its inhibitory activity for the self-cleavage of hammerhead ribozyme. *Life-Basel.* 12, 1689.
50. Stephenson, J. D., M. Popović, …, M. A. Ditzler. 2016. Evolution of ribozymes in the presence of a mineral surface. *RNA.* 22:1893–1901.
51. Swadling, J. B., D. W. Wright, …, P. V. Coveney. 2015. Structure, dynamics, and function of the hammerhead ribozyme in bulk water and at a clay mineral surface from replica exchange molecular dynamics. *Langmuir.* 31:2493–2501.
52. Saha, R., S. Verbanic, and I. A. Chen. 2018. Lipid vesicles chaperone an encapsulated RNA aptamer. *Nat. Commun.* 9:2313.
53. Peng, H., A. Lelievre, …, I. A. Chen. 2022. Vesicle encapsulation stabilizes intermolecular association and structure formation of functional RNA and DNA. *Curr. Biol.* 32:86–96.e6.
54. Desai, R., D. Kilburn, …, S. A. Woodson. 2014. Increased ribozyme activity in crowded solutions. *J. Biol. Chem.* 289:2972–2977.
55. Lai, Y.-C., Z. Liu, and I. A. Chen. 2021. Encapsulation of ribozymes inside model protocells leads to faster evolutionary adaptation. *Proc. Natl. Acad. Sci. USA.* 118, e2025054118.
56. Saha, R., A. Pohorille, and I. A. Chen. 2014. Molecular crowding and early evolution. *Orig. Life Evol. Biosph.* 44:319–324.
57. Babendure, J. R., S. R. Adams, and R. Y. Tsien. 2003. Aptamers switch on fluorescence of triphenylmethane dyes. *J. Am. Chem. Soc.* 125:14716–14717.
58. Sciascia, L., M. L. Turco Liveri, and M. Merli. 2011. Kinetic and equilibrium studies for the adsorption of acid nucleic bases onto K10 montmorillonite. *Appl. Clay Sci.* 53:657–668.
59. Degenhardt, J., and A. J. McQuillan. 1999. In situ ATR-FTIR spectroscopic study of adsorption of perchlorate, sulfate, and thiosulfate ions onto chromium(III) oxide hydroxide thin films. *Langmuir.* 15:4595–4602.
60. Schulz, M. N., J. Landström, and R. E. Hubbard. 2013. MTSA–a Matlab program to fit thermal shift data. *Anal. Biochem.* 433:43–47.
61. Lakowicz, J. R. 2006. Principles of Fluorescence Spectroscopy. Springer.
62. Flinders, J., S. C. DeFina, …, T. Dieckmann. 2004. Recognition of planar and nonplanar ligands in the malachite green-RNA aptamer complex. *Chembiochem.* 5:62–72.
63. Delaglio, F., S. Grzesiek, …, A. Bax. 1995. NMRPipe: a multidimensional spectral processing system based on UNIX pipes. *J. Biomol. NMR.* 6:277–293.
64. Johnson, B. A. 2004. Using NMRView to visualize and analyze the NMR spectra of macromolecules. *Methods Mol. Biol.* 278:313–352.
65. Swadling, J. B., J. L. Suter, …, P. V. Coveney. 2013. Influence of surface chemistry and charge on mineral–RNA interactions. *Langmuir.* 29:1573–1583.
66. Zatta, L., L. P. Ramos, and F. Wypych. 2013. Acid-activated montmorillonites as heterogeneous catalysts for the esterification of lauric acid with methanol. *Appl. Clay Sci.* 80–81:236–244.
67. Shimizu, K. I., T. Higuchi, …, A. Satsuma. 2008. Characterization of Lewis acidity of cation-exchanged montmorillonite K-10 clay as effective heterogeneous catalyst for acetylation of alcohol. *J. Mol. Catal. Chem.* 284:89–96.
68. Török, B., G. Szöllösi, …, M. Bartók. 1998. Preparation, characterization and application of K-10 montmorillonite modified with chiral ammonium halides. *Mol. Cryst. Liq. Cryst. A.* 311:289–294.
69. Mathew, D. C., and Z. Luthey-Schulten. 2010. Influence of montmorillonite on nucleotide oligomerization reactions: a molecular dynamics study. *Orig. Life Evol. Biosph.* 40:303–317.
70. Poly, F., C. Chenu, …, L. Jocteur Monrozier. 2000. Differences between linear chromosomal and supercoiled plasmid DNA in their mechanisms and extent of adsorption on clay minerals. *Langmuir.* 16:1233–1238.
71. Baugh, C., D. Grate, and C. Wilson. 2000. 2.8 Å Crystal structure of the Malachite Green aptamer. *J. Mol. Biol.* 301:117–128.
72. Bernard Da Costa, J., and T. Dieckmann. 2011. Entropy and Mg^{2+} control ligand affinity and specificity in the malachite green binding RNA aptamer. *Mol. Biosyst.* 7:2156–2163.
73. Heus, H. A., and A. Pardi. 1991. Structural features that give rise to the unusual stability of RNA hairpins containing GNRA loops. *Science.* 253:191–194.
74. Jucker, F. M., H. A. Heus, …, A. Pardi. 1996. A network of heterogeneous hydrogen bonds in GNRA tetraloops. *J. Mol. Biol.* 264:968–980.
75. Varani, G. 1995. Exceptionally stable nucleic acid hairpins. *Annu. Rev. Biophys. Biomol. Struct.* 24:379–404.